INTERNATIONAL JOURNAL FOR NUMERICAL METHODS IN FLUIDS, VOL. 12, 305–322 (1991)

AN UPWIND FINITE ELEMENT SCHEME FOR HIGH-REYNOLDS-NUMBER FLOWS

MASAHISA TABATA AND SHOICHI FUJIMA

Department of Computer Science and Information-Mathematics, University of Electro-Communications, 1-5-1 Chofugaoka, Chofu, Tokyo 182, Japan

SUMMARY

A new upwind finite element scheme for the incompressible Navier–Stokes equations at high Reynolds number is presented. The idea of the upwind technique is based on the choice of upwind and downwind points. This scheme can approximate the convection term to third-order accuracy when these points are located at suitable positions. From the practical viewpoint of computation, the algorithm of the pressure Poisson equation procedure is adopted in the framework of the finite element method. Numerical results of flow problems in a cavity and past a circular cylinder show excellent dependence of the solutions on the Reynolds number. The influence of rounding errors causing Karman vortex shedding is also discussed in the latter problem.

KEY WORDS Upwind finite element method Navier–Stokes equations Upwind and downwind points High-Reynolds-number flows Influence of rounding errors

INTRODUCTION

In the development of schemes for given problems, we have to pay attention to the stability. The stability, however, is not always sufficient for the computation of practical problems. There are some problems where other properties may become as important as the stability. In the computation of flow problems at high Reynolds numbers the sensitivity with respect to the Reynolds number is one of those properties. That is, the scheme is expected to produce solutions which show a clear dependence on the Reynolds number.

As is well known, the Galerkin finite element approximation leads to instability for problems at high Reynolds numbers. This is caused by the fact that the derived scheme is a central-difference-type approximation to the convection term. Thus the question is how to approximate the convection term. Several first-order upwind approximations have been proposed.[1–3] They are stable but their sensitivity to the Reynolds number is not always good on account of the additional viscosity included. In the finite difference field, upwind approximations with third-order accuracy have been developed and their good sensitivity to the Reynolds number has been recognized.[4–7] Recently, Kondo *et al.*[8] have presented a finite element scheme with third-order upwinding based on the Petrov–Galerkin method.[9] We refer to Reference 10 for the analysis of discontinuous upwind finite element schemes and to References 11 and 12 for the computation of high-Reynolds-number flow problems by the streamline upwind/Petrov–Galerkin formulation.[13,14]

In this paper we present a new upwind finite element scheme for the incompressible Navier–Stokes equations. Our upwinding technique is based on the choice of upwind and

0271–2091/91/040305–18$09.00

Received 28 August 1989
Revised 27 February 1990

downwind points. This technique has been developed by one of the authors[15] to the first-order accuracy and extended by Bristeau *et al.*[16] (see Remark 3). Our scheme approximates the convection term to third-order accuracy when upwind and downwind points coincide with nodal points. In this sense we may regard it as an extension to the finite element method of the third-order upwind finite difference approximation developed by Kawamura *et al.*[6] For the time integration we employ the forward Euler method and use the consistent discretized pressure Poisson equation[17,18] procedure in solving the system of linear equations obtained. As a result, the size of the linear equations to be solved is reduced to the number of degrees of freedom of the pressure.

In order to obtain better solutions of flow problems at high Reynolds numbers, the refined subdivision of boundary layers is no less important than the good approximation of the convection term. In the finite difference method, numerical grid generation[19] is often used to obtain body-fitting curvilinear co-ordinates. One of the advantages of the finite element method is its geometric flexibility. By using this advantage we can easily decompose the boundary layer as we like. In our method we do not need to use systematic grid generation.

We present numerical results for two problems to show the efficiency of our scheme. One is the flow problem in a cavity at $Re=1000$ and 10 000. The other is the flow problem past a circular cylinder at $Re=10$, 100, 1000 and 10 000. In the latter problem we also discuss the influence of rounding errors, which are the cause of Karman vortex shedding.

INCOMPRESSIBLE NAVIER–STOKES EQUATIONS

Let Ω be a bounded domain in $\mathbb{R}^2$ and T be a positive constant. Consider the incompressible Navier–Stokes equations in $\Omega\times(0, T)$:

$$\partial u/\partial t+(u\cdot\operatorname{grad})u+\operatorname{grad} p=(1/Re)\nabla^2 u+f, \tag{1a}$$

$$\operatorname{div} u=0, \tag{1b}$$

where $u=(u_1, u_2)$ is the velocity, p is the pressure, Re is the Reynolds number and $f=(f_1, f_2)$ is the outer force. Equations (1) are discretized in time as follows:

$$(u^{n+1}-u^n)/\Delta t+u^n\cdot\operatorname{grad} u^n+\operatorname{grad} p^n=(1/Re)\nabla^2 u^n+f^n, \tag{2a}$$

$$\operatorname{div} u^{n+1}=0, \tag{2b}$$

where Δt is a time increment and u^n, for example, denotes the value of u at time $n\Delta t$. For the space discretization we employ the standard mixed finite element formulation, except for the time difference term and the convection term. For the time difference term we use the lumping technique. For the convection term we adopt a new upwind approximation $(u^n\cdot\operatorname{grad} u^n)_h$ defined later. We note that the bilinear form

$$a_0(u, v)=(2/Re)\int_\Omega \sum_{i,j=1}^{2} D_{ij}(u)D_{ij}(v)\,dx,$$

$$D_{ij}(u)=(\partial u_i/\partial x_j+\partial u_j/\partial x_i)/2$$

is employed for the viscosity term in order to treat the stress boundary condition easily. We use a variant of the Hood–Taylor element, namely the Bercovier–Pironneau element.[20,21] That is, we divide the domain into a union of triangles and further divide each triangle into four congruent triangles. Pressure p is approximated by the P1-element on large triangles and velocity u is

approximated by the P1-element on small triangles (see Figure 1). Throughout this paper we assume the triangulation is regular,[22] i.e. the minimum angle condition.

Equations (2) are reduced to a system of linear equations:

$$(\bar{M}/\Delta t)u_h^{n+1} + B^{\mathrm{T}}p_h^n = r^n, \tag{3a}$$

$$Bu_h^{n+1} = s^n, \tag{3b}$$

where $\bar{M}$ is the lumped mass matrix, B is the 'divergence' matrix and r^n and s^n are known vectors. We can solve equations (3) by

$$(B\bar{M}^{-1}B^{\mathrm{T}})p_h^n = B\bar{M}^{-1}r^n - s^n/\Delta t. \tag{4}$$

Matrix $B\bar{M}^{-1}B^{\mathrm{T}}$ is an approximation of the Laplace operator and equation (4) is called the consistent discretized pressure Poisson equation by Gresho *et al.*[17,18] Velocity u_h^{n+1} is solved by equation (3a) afterwards. Thus the main part of the computation in our scheme is to solve a small-size system of linear equations (4) in pressure. We note that $B\bar{M}^{-1}B^{\mathrm{T}}$ is a band matrix since matrix $\bar{M}$ is diagonal.

Proposition 1

Equation (4) is uniquely solvable.

Proof. Let q_h be a solution of

$$(B\bar{M}^{-1}B^{\mathrm{T}})q_h = 0.$$

Then we have

$$(\bar{M}^{-1}B^{\mathrm{T}}q_h,\ B^{\mathrm{T}}q_h) = 0,$$

which implies

$$B^{\mathrm{T}}q_h = 0.$$

Since the Bercovier–Pironneau element satisfies the inf–sup condition under the assumption of regular triangulation,[23,24] it holds that

$$\|B^{\mathrm{T}}q_h\| \geq \beta \|q_h\|,$$

where β is a positive constant of the inf–sup condition. Hence we have

$$q_h = 0.$$

Remark 1

The above proof is valid even if the coefficient β is dependent on h; that is, the inf–sup condition is not necessary for the unique solvability. In fact, the unique solvability of equation (4) can be

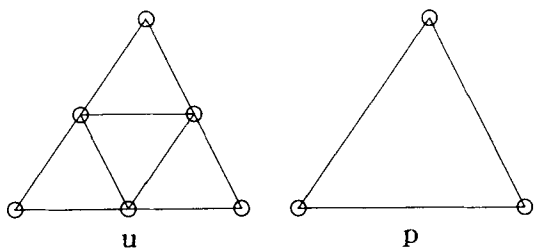

Figure 1. Bercovier–Pironneau element

proved without the assumption of regular triangulation. This proposition assures that no spurious pressure modes appear.

POTENTIAL THIRD-ORDER UPWIND APPROXIMATION

Let $b:\Omega \to \mathbb{R}^2$ be a given velocity and $v:\Omega \to \mathbb{R}$ be a scalar function. We derive the approximation $(b\cdot \operatorname{grad} v)_h$ to $(b\cdot \operatorname{grad})v$. Let O be a nodal point. Assume that $b(\mathrm{O})$ does not vanish. We introduce the orthogonal local co-ordinate system (ξ, η) with origin O and unit ξ-vector $b(\mathrm{O})/|b(\mathrm{O})|$. Then the convection term is written as

$$(b\cdot \operatorname{grad} v)(\mathrm{O}) = |b(\mathrm{O})|\,\partial v/\partial \xi(\mathrm{O}). \tag{5}$$

We choose four points U, W, D and B on the ξ-axis such that U is an upwind point of O with respect to the flow b, W is a further upwind point, D is a downwind point and B is a further downwind point (see Figure 2). The method of practical choice of these points will be presented in the following section. Let h be the representative element length around O. We set

$$h = \text{length OU}.$$

We denote by $\xi_{\mathrm{P}} = \xi'_{\mathrm{P}} h$ the ξ-co-ordinate of $\mathrm{P}\in\{\mathrm{W}, \mathrm{U}, \mathrm{O}, \mathrm{D}, \mathrm{B}\}$ ($\xi'_{\mathrm{O}}=0$, $\xi'_{\mathrm{U}}=-1$). We approximate $\partial v/\partial\xi(\mathrm{O})$ by the values of v at five points W, U, O, D and B as follows:

$$(b\cdot \operatorname{grad} v)_h(\mathrm{O}) = |b(\mathrm{O})| \sum_{\mathrm{P}\in\{\mathrm{W},\mathrm{U},\mathrm{O},\mathrm{D},\mathrm{B}\}} \gamma_{\mathrm{P}} v(\mathrm{P})/h, \tag{6}$$

where

$$\gamma_{\mathrm{P}} = \left(\prod_{\mathrm{Q}\neq \mathrm{P},\mathrm{O}} (\xi'_{\mathrm{O}} - \xi'_{\mathrm{Q}}) + \alpha \right) \Big/ \prod_{\mathrm{Q}\neq \mathrm{P}} (\xi'_{\mathrm{P}} - \xi'_{\mathrm{Q}}), \qquad \mathrm{P}\neq \mathrm{O},$$

$$\gamma_{\mathrm{O}} = -\sum_{\mathrm{Q}\neq \mathrm{O}} \gamma_{\mathrm{Q}}$$

and α is a non-negative parameter.

Proposition 2

Suppose that there exist positive constants c_1 and c_2 independent of h such that

$$c_1 h \leqslant \xi_{\mathrm{B}} - \xi_{\mathrm{D}},\quad \xi_{\mathrm{D}} - \xi_{\mathrm{O}},\quad \xi_{\mathrm{O}} - \xi_{\mathrm{U}},\quad \xi_{\mathrm{U}} - \xi_{\mathrm{W}} \leqslant c_2 h. \tag{7}$$

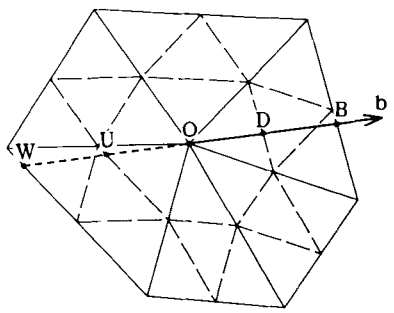

Figure 2. Velocity $b(\mathrm{O})$ and points W, U, O, D and B

Then we have for every sufficiently smooth function v,

$$(b\cdot\operatorname{grad} v)_h(\mathrm{O})=(b\cdot\operatorname{grad} v)(\mathrm{O})+\alpha|b(\mathrm{O})|\partial^4 v/\partial\xi^4(\mathrm{O})h^3/4!+O(h^4). \tag{8}$$

Proof. We set $\gamma_{\mathrm{P}}=\gamma_{\mathrm{P}}^1+\gamma_{\mathrm{P}}^2$, where

$$\gamma_{\mathrm{P}}^1=\prod_{\mathrm{Q}\neq\mathrm{P},\mathrm{O}}(\xi'_{\mathrm{O}}-\xi'_{\mathrm{Q}})\Big/\prod_{\mathrm{Q}\neq\mathrm{P}}(\xi'_{\mathrm{P}}-\xi'_{\mathrm{Q}}),\qquad \mathrm{P}\neq\mathrm{O},$$

$$\gamma_{\mathrm{O}}^1=-\sum_{\mathrm{Q}\neq\mathrm{O}}\gamma_{\mathrm{Q}}^1,$$

$$\gamma_{\mathrm{P}}^2=\alpha\Big/\prod_{\mathrm{Q}\neq\mathrm{P}}(\xi'_{\mathrm{P}}-\xi'_{\mathrm{Q}}).$$

Then we have

$$\sum_{\mathrm{P}\in\{\mathrm{W},\mathrm{U},\mathrm{O},\mathrm{D},\mathrm{B}\}}\gamma_{\mathrm{P}}^1 v(\mathrm{P})/h=\mathrm{d}P_4/\mathrm{d}\xi(\mathrm{O})=\partial v/\partial\xi(\mathrm{O})+O(h^4),$$

$$\sum_{\mathrm{P}\in\{\mathrm{W},\mathrm{U},\mathrm{O},\mathrm{D},\mathrm{B}\}}\gamma_{\mathrm{P}}^2 v(\mathrm{P})/h=\alpha h^3 v[\mathrm{W},\mathrm{U},\mathrm{O},\mathrm{D},\mathrm{B}]=\alpha h^3\partial^4 v/\partial\xi^4(\mathrm{O})+O(h^4),$$

where $P_4(\xi; v(\mathrm{P}), \mathrm{P}=\mathrm{W},\mathrm{U},\mathrm{O},\mathrm{D},\mathrm{B})$ is the fourth-order Lagrange interpolation and $v[\mathrm{W},\mathrm{U},\mathrm{O},\mathrm{D},\mathrm{B}]$ is the fourth-order divided difference. Hence we obtain (8).

Remark 2

(i) When $\alpha=0$, equation (6) is the fourth-order central approximation.

(ii) Equation (6) becomes the third-order Leonard-type[4] upwind approximation using W, U, O and D when

$$\alpha=-\prod_{\mathrm{Q}\neq\mathrm{B},\mathrm{O}}(\xi'_{\mathrm{O}}-\xi'_{\mathrm{Q}}). \tag{9}$$

We have reported this case briefly in a previous paper.[25]

(iii) Equation (6) becomes the third-order Leonard-type[4] upwind approximation using W, U, O and B when

$$\alpha=-\prod_{\mathrm{Q}\neq\mathrm{D},\mathrm{O}}(\xi'_{\mathrm{O}}-\xi'_{\mathrm{Q}}). \tag{10}$$

(iv) Suppose the case where W, U, O, D and B are located uniformly; that is, the lengths of BD, DO, OU and UW are equal to h. Then (6) becomes the third-order Kawamura-type approximation when $\alpha=6$. Note that $\alpha=2$ in (9) and $\alpha=4$ in (10) when W, U, O, D and B are located uniformly.

(v) α is the parameter which stabilizes the scheme. From (8) we set $\alpha'=\alpha/4!$. We choose α' between 0 and $\frac{1}{4}$ (i.e. $\alpha\in[0, 6]$) from the above discussion.

Remark 3

(i) In a previous paper[15] we presented a first-order upwind finite element approximation to (5):

$$b(\mathrm{O})\cdot\operatorname{grad} v_h(T_{\mathrm{O}}), \tag{11}$$

where T_{O}, the upwind element of O, is defined as an element such that O is a vertex of T_{O} and the

half-line starting from O with direction $-b(\mathrm{O})$ crosses T_{O}. Since we use the piecewise linear element, grad $v_h(T_{\mathrm{O}})$ is constant and (11) is equal to

$$|b(\mathrm{O})|(v_h(\mathrm{O})-v_h(\mathrm{U}))/h. \tag{12}$$

Hence (6) is a higher-order extension of (11).

(ii) Bristeau *et al.*[16] extended (12) to approximate (5) by three points, W, U and O (the choice of W is a little different). Then the main truncation error in (8) becomes const. $\times |b(\mathrm{O})|\partial^3 v/\partial\xi^3(\mathrm{O})h^2$.

In the weak formulation we approximate the trilinear form

$$a_1(w, u, v)=\sum_{i=1}^{2}\int_{\Omega}(w\cdot\mathrm{grad})u_i v_i\,\mathrm{d}x$$

by

$$a_1^h(w_h, u_h, v_h)=\sum_{i=1}^{2}\sum_{\mathrm{P}}(w_h\cdot\mathrm{grad}\,u_{hi})_h(\mathrm{P})v_{hi}(\mathrm{P})\,\mathrm{mes}\,D_{\mathrm{P}}, \tag{13}$$

where P runs over all nodal points and mes D_{P} is the measure of the barycentric domain[2] D_{P} around P. Since we use the piecewise linear element, the values of u_h at upwind or downwind points are obtained by the linear interpolation of nodal values. Therefore (13) is not of third-order accuracy in general, but it is when these points are located suitably, e.g. when they coincide with nodal points. In the neighbourhood of the boundary where we cannot find the points W or B, we employ the first-order upwind approximation (12) or the Leonard-type upwind approximation (9) in place of (6).

CHOICE OF UPWIND AND DOWNWIND POINTS

We denote by $\mathscr{F}$ the collection of all vertices and all (closed) sides of (small) triangles. Let F be an element in $\mathscr{F}$. We denote by $\mathscr{C}(F)$ all elements in $\mathscr{F}$ which have no intersection with F:

$$\mathscr{C}(F)=\{A\in\mathscr{F};\quad A\cap F=\varnothing\}.$$

Let P be a point on the ξ-axis. We denote by $l_-(\mathrm{P})$ the half-line starting from P in the $-\xi$-direction. The upwind point $\mathrm{U}(\xi_{\mathrm{U}}, 0)$ is defined by

$$\xi_{\mathrm{U}}=\max\{\xi;\ \mathrm{P}(\xi,0)\in F\cap l_-(\mathrm{O}),\ F\in\mathscr{C}(\mathrm{O})\}.$$

We denote by F_{U} the element in $\mathscr{C}(\mathrm{O})$ including U:

$$\mathrm{U}\in F_{\mathrm{U}}\in\mathscr{C}(\mathrm{O}).$$

Such an element can be found uniquely unless $\mathrm{U}\in\mathscr{F}$, where we set $F_{\mathrm{U}}=\mathrm{U}$. The other upwind point $\mathrm{W}(\xi_{\mathrm{W}}, 0)$ is defined by

$$\xi_{\mathrm{W}}=\max\{\xi;\ \mathrm{P}(\xi,0)\in F\cap l_-(\mathrm{U}),\ F\in\mathscr{C}(F_{\mathrm{U}})\}.$$

The downwind points D and B are defined as upwind points U and W corresponding to $-b(\mathrm{O})$.

By virtue of the assumption that the subdivision is regular, we have:

Proposition 3

The upwind and downwind points chosen as above satisfy relation (7).

NUMERICAL RESULTS

We solve two model flow problems. In the following the outer force $f=0$ and the initial value $u=0$. The boundary condition is shown in each problem. We solve the Navier–Stokes equations evolutionally by (3).

Flow in a cavity

The problem is explained in Figure 3. Figure 4 shows the division of the domain. Each side is divided into 24 non-uniform intervals (the minimum element size of pressure is $h_p \simeq 0{\cdot}014$) and the total number of elements (of p) is 1152. We choose the value α given in (9). The time increment Δt is 0·0075 in the case of $Re=1000$. This value was selected experimentally and also on the basis of the CFL condition by considering that the phenomena are convection-dominated for high-Reynolds-number flows. In the case of $Re=10\,000$ we decreased the time increment a little, $\Delta t=0{\cdot}005$, since the solution had not become stationary. With this Δt the solution became

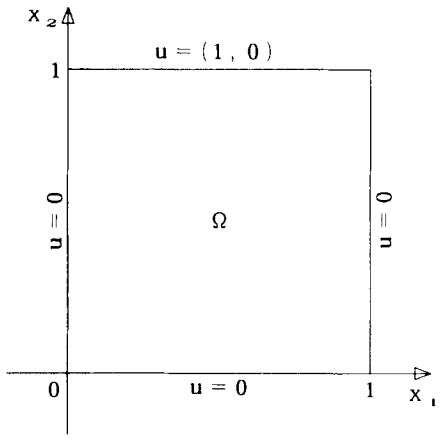

Figure 3. Flow in a cavity

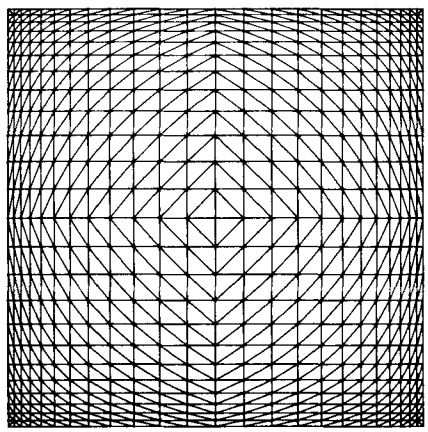

Figure 4. Division of the domain

almost stationary but a slight oscillation remained. Figures 5 ($Re=1000$) and 6 ($Re=10000$) show the streamlines of the stationary solution (almost stationary solution for $Re=10000$) and the graphs of $u_1(0{\cdot}5,\cdot)$. In these figures we compare our results with others obtained by:

(a) Ghia *et al.*,[26] FDM without upwinding, 128×128 ($Re=1000$), 256×256 ($Re=10000$)
(b) Nallasamy and Prasad,[27] FDM with first-order upwinding, 50×50
(c) Takemoto *et al.*,[5] FDM with third-order upwinding, 100×100
(d) Kondo *et al.*,[8] FEM with third-order upwinding, 40×40 ($Re=1000$), 44×44 ($Re=10000$)
(e) ourselves, FEM with first-order upwinding (11), 16×16 (a result computed this time in order to be compared with the present scheme)

where $N\times N$ means that each side is divided into N segments.

We can observe the good agreement between our results and those obtained by Ghia *et al.* Note that we used a relatively rough mesh division. We omit the result of the FEM with first-order upwinding in Figure 6 since it is almost the same as in Figure 5. This means that the dependence of first-order upwinding on the Reynolds number is not very good. On the other hand, as seen from Figures 5 and 6, the present scheme produces solutions having a good dependence on the Reynolds number.

Remark 4

Our subdivision is 24×24 in p, which amounts to 48×48 in u. As explained, the main computation of our scheme is to solve the system of linear equations (4) in p. Therefore it may not be so unfair to take $N=24$ for our subdivision in comparing the results with the others.

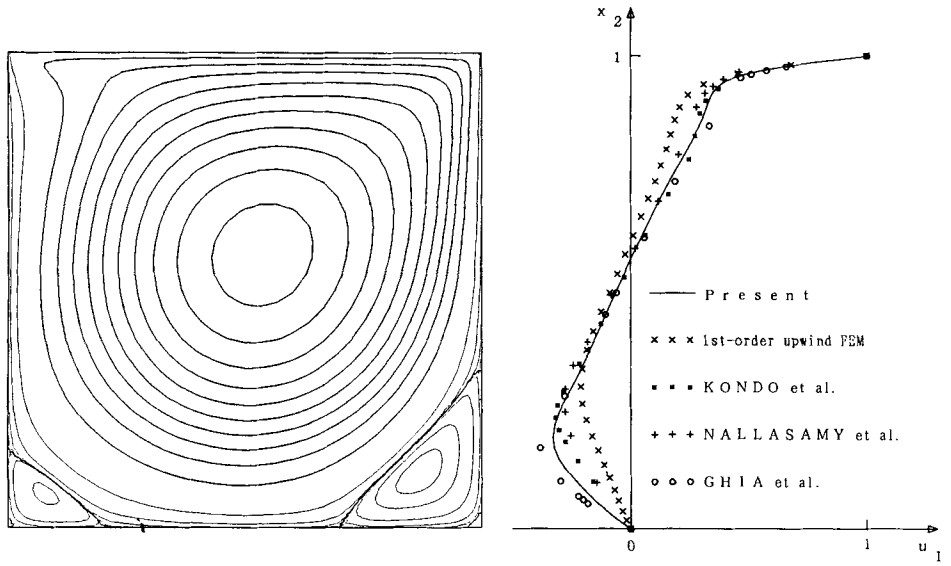

Figure 5. Streamlines and graph of $u_1(0{\cdot}5,\cdot)$; $Re=1000$

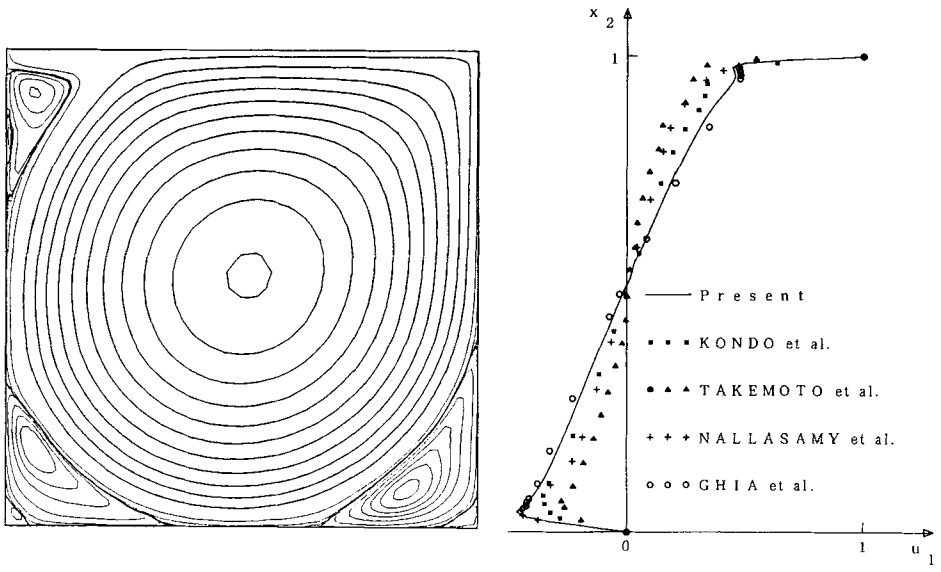

Figure 6. Streamlines and graph of $u_1(0{\cdot}5, \cdot)$; $Re = 10\,000$

Flow past a circular cylinder

The problem is explained in Figure 7, where

$$\tau_i = \sum_{j=1}^{2} \{-p\delta_{ij} + (2/Re)D_{ij}(u)\} n_j, \quad i = 1, 2,$$

and $n = (n_1, n_2)$ is the unit outward normal to the boundary. At the origin there exists a circular cylinder with unit diameter. The computational domain is $[-7{\cdot}5, 22{\cdot}5] \times [-7{\cdot}5, 7{\cdot}5]$. The total number of elements (of p) in Figure 7 is 2334 and the minimum element size of velocity is $h_u \simeq 0{\cdot}028$. We set $\alpha' = 0{\cdot}08$. We chose $\Delta t = 0{\cdot}002$ ($Re = 10$) and $\Delta t = 0{\cdot}01$ ($Re = 100$) in consideration of the finite difference stability condition of the heat equation, $\Delta t \leqslant Re\, h_u^2/4$, since the phenomena are diffusion-dominated for low-Reynolds-number flows. Figures 8 ($Re = 10$) and 9 ($Re = 100$) depict the time histories of drag coefficient C_D and lift coefficient C_L. C_L is nearly zero in Figure 8. At $Re = 10$ a stationary solution was obtained (Figure 10). At $Re = 100$ we observed Karman vortex shedding (Figure 11). For the computation at higher Reynolds numbers we used more refined subdivisions. The subdivision for $Re = 1000$ is shown in Figure 12. The total number of elements (of p) is 4320. The nodal point number (of p) on the cylinder increased to 64 from 48 and the boundary layer was subdivided into smaller elements. $h_u \simeq 0{\cdot}011$ and it is attained as the lengths in the radial direction of elements nearest to the cylinder. The subdivision for $Re = 10\,000$ was similar to the one for $Re = 1000$ except for the location of nodal points; that is, the total number of elements and the topology of the subdivision were same but the layer was subdivided more finely by moving the nodal points towards the surface of the cylinder and $h_u \simeq 0{\cdot}003$. Note that the decreasing rate of h_u is nearly equal to $1/\sqrt{(Re)}$, the theoretical decreasing rate of boundary layer thickness. We chose $\Delta t = 0{\cdot}01$ ($Re = 1000$) and $\Delta t = 0{\cdot}0075$ ($Re = 10\,000$) in consideration of the CFL condition (see also Remark 5 below). At $Re = 10\,000$ we increased the value of α' to 0·12 since the solution had diverged for $\alpha' = 0{\cdot}08$. At present we have not obtained

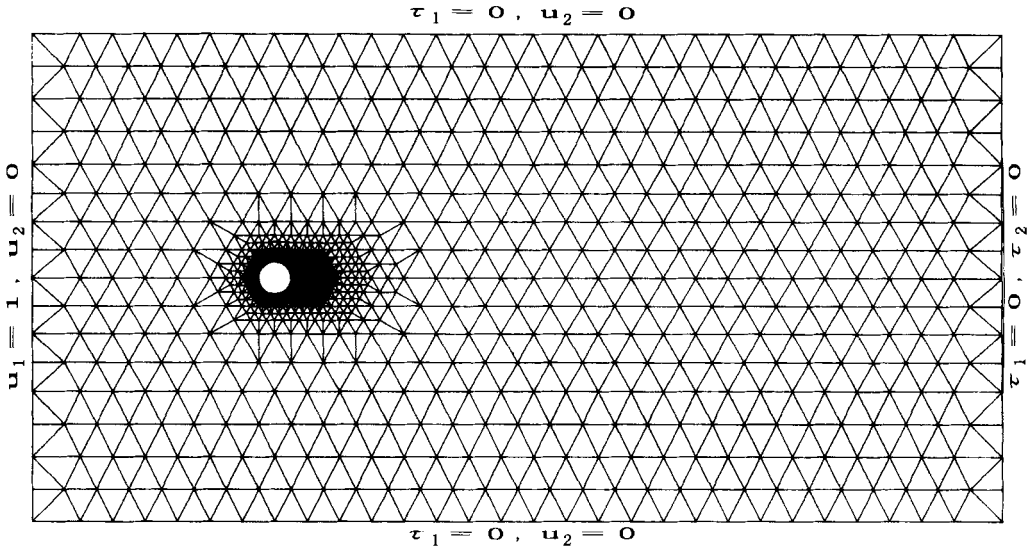

Figure 7. Flow past a circular cylinder

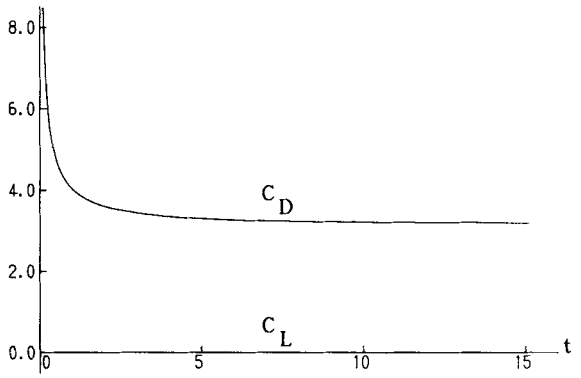

Figure 8. Time histories of C_D and C_L; $Re = 10$

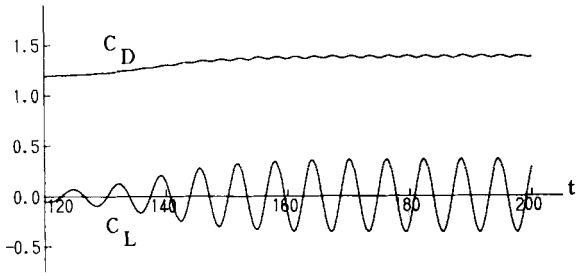

Figure 9. Time histories of C_D and C_L; $Re = 100$

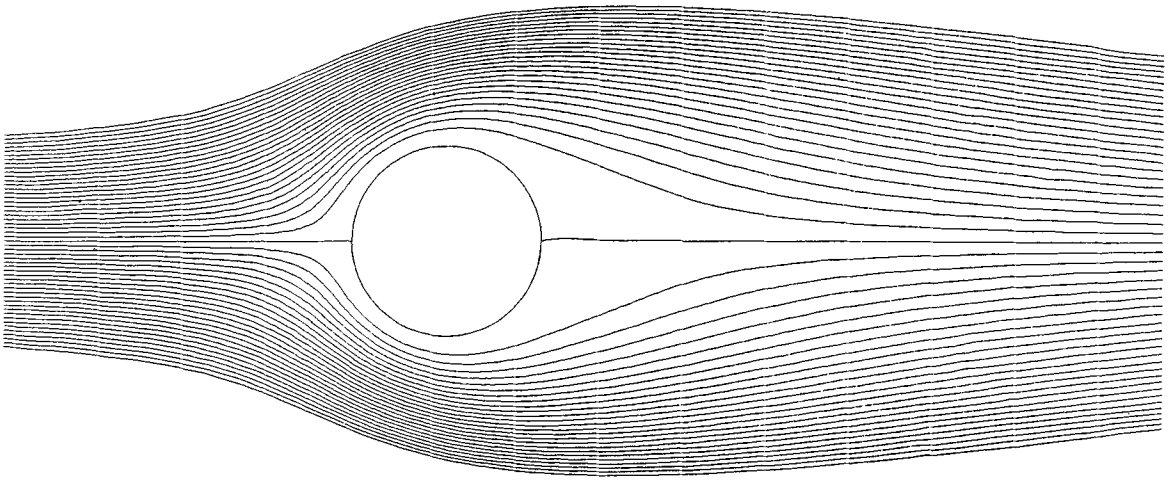

Figure 10. Stationary solution; $Re = 10$

the critical value of α'. To find it is an open problem. Figures 13 ($Re = 1000$, $\alpha' = 0{\cdot}08$) and 14 ($Re = 10\,000$, $\alpha' = 0{\cdot}12$) depict the time histories of C_D and C_L. In both cases we observed Karman vortex shedding. Figure 15 ($Re = 10\,000$) shows the streamlines at a time $t = 59{\cdot}25$. The detailed structure near the cylinder is seen in Figure 16. The qualitative agreement between the results of the present computation and experiment[28] is good.

Remark 5

When $Re = 10\,000$, Δt does not satisfy the CFL condition for the above h_u and the representative velocity. However, near the surface of the cylinder the minimum element size in the angular direction is about 0·016. Therefore, if the velocity in the radial direction in the layer is not too large, the CFL condition will be satisfied. In this subdivision the aspect ratio of the angular direction to the radial direction of elements near the cylinder becomes quite large (about 11). This ratio is not very desirable from the viewpoint of regular triangulation. In the subdivision at $Re = 1000$ the ratio is about 3 near the cylinder and about 4 in the whole domain.

INFLUENCE OF ROUNDING ERRORS

In the computation of flow past a circular cylinder, the scheme as well as the mesh division and the input data were symmetric with respect to the x_1-axis. Therefore, if all computations had been done exactly, the solutions should have been symmetric at any time. However, we obtained asymmetric solutions (Karman vortex shedding) at $Re = 100$, 1000 and 10 000. This must be caused by rounding errors in the process of computation. In order to examine this influence, we computed the same problem ($Re = 100$) in double-precision. Figure 17 shows the time histories of C_D and C_L by the single-precision computation as well as the double-precision computation. From this figure we see clearly the difference in time when the stable Karman vortex shedding appears. In single-precision each operation includes greater rounding errors and the Karman vortex shedding appears earlier. The states of Karman vortex shedding in both computations are

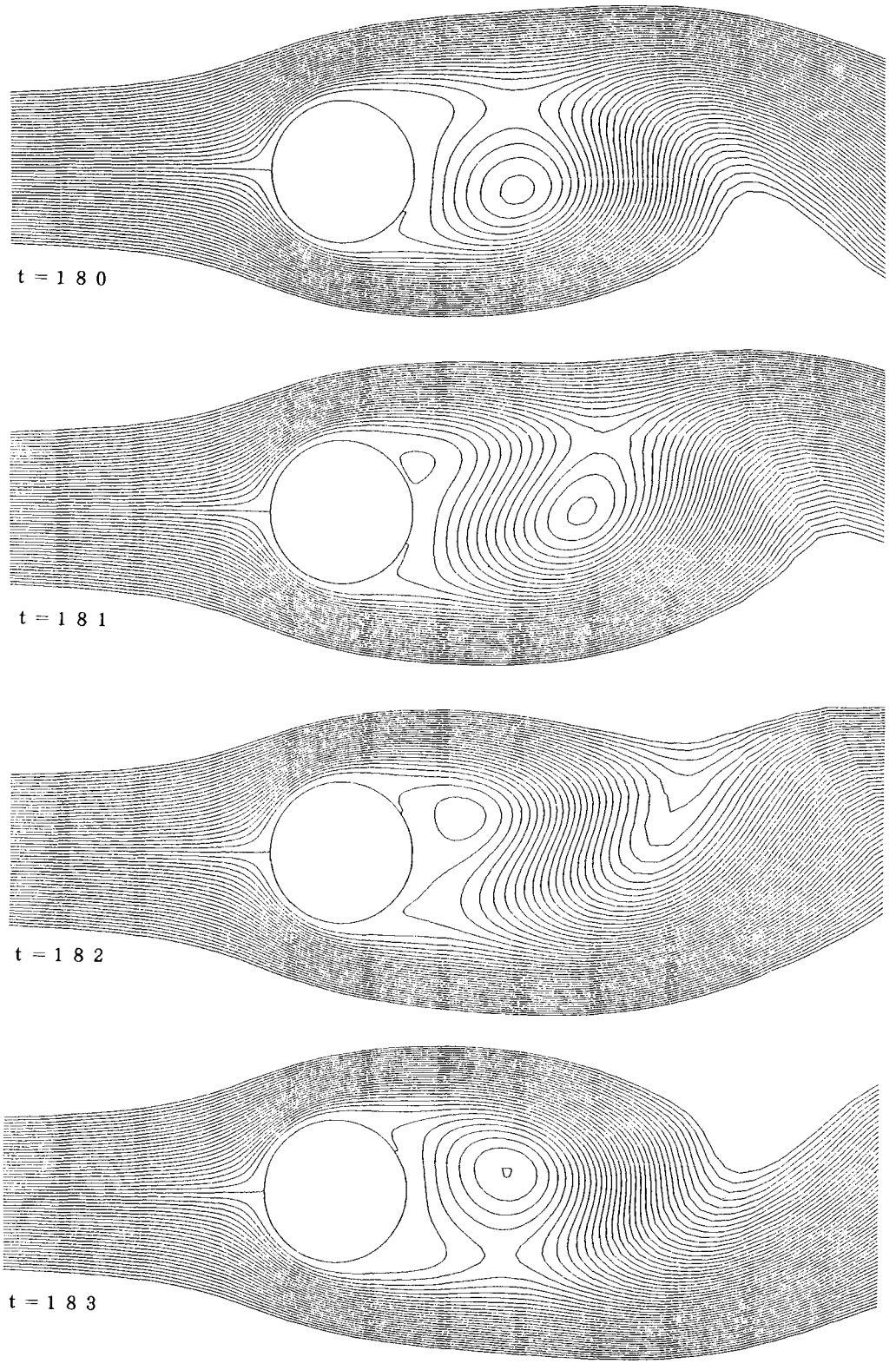

Figure 11. (Continued)

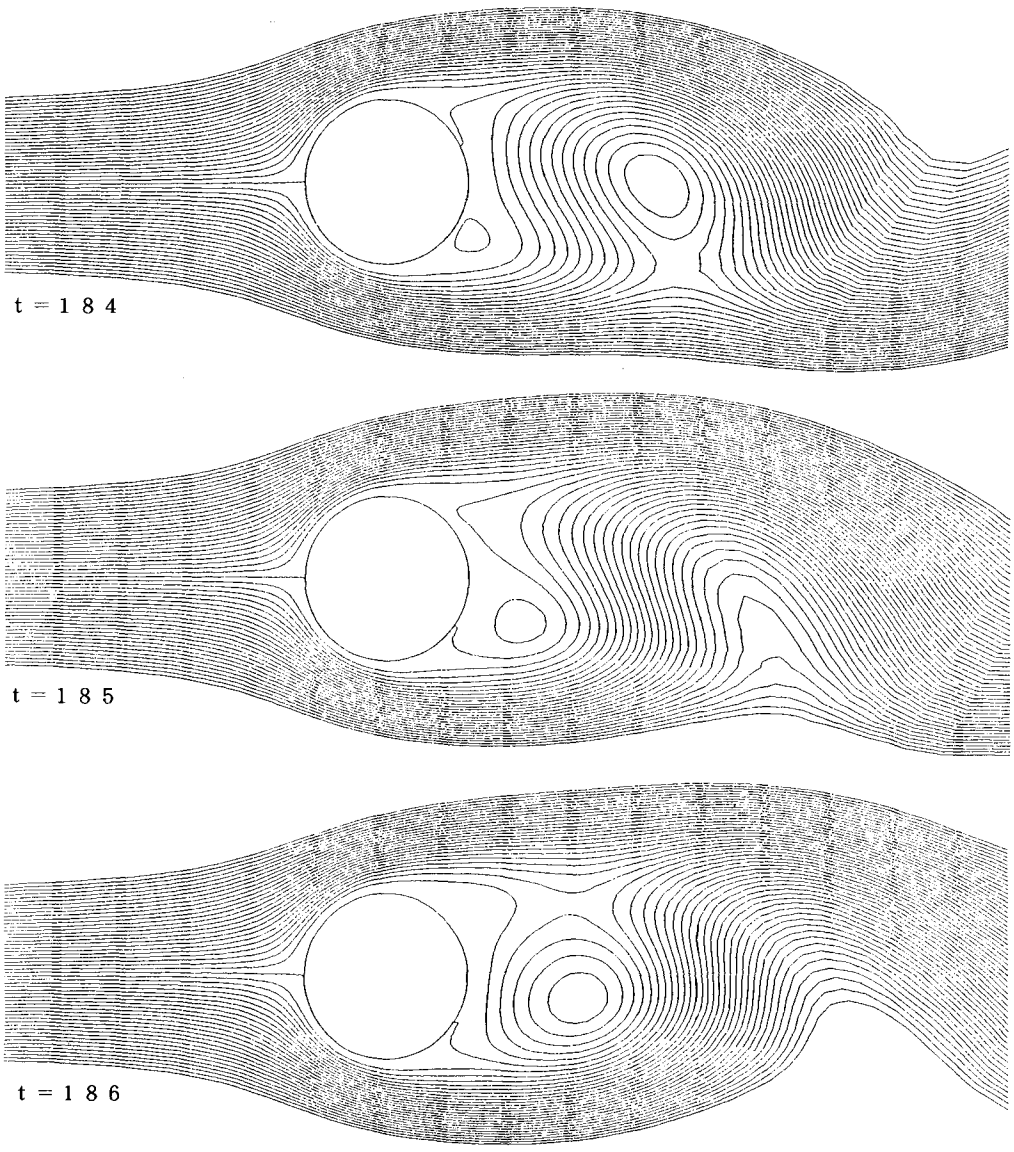

Figure 11. Karman vortex shedding; $Re = 100$

stable and almost identical except for the phase lag. Figure 18 shows the variations of velocity and pressure at each step:

$$\log_{10}(\|u^{n+1}-u^n\|/U\Delta t), \qquad \log_{10}(\|p^{n+1}-p^n\|/P\Delta t),$$

where U and P are representative velocity and pressure and $\|\cdot\|$ denotes the maximum norm. Initially the variations decrease and the solutions seem to converge to a stationary solution, especially in the double-precision computation at about $t = 200$. However, the variations increase

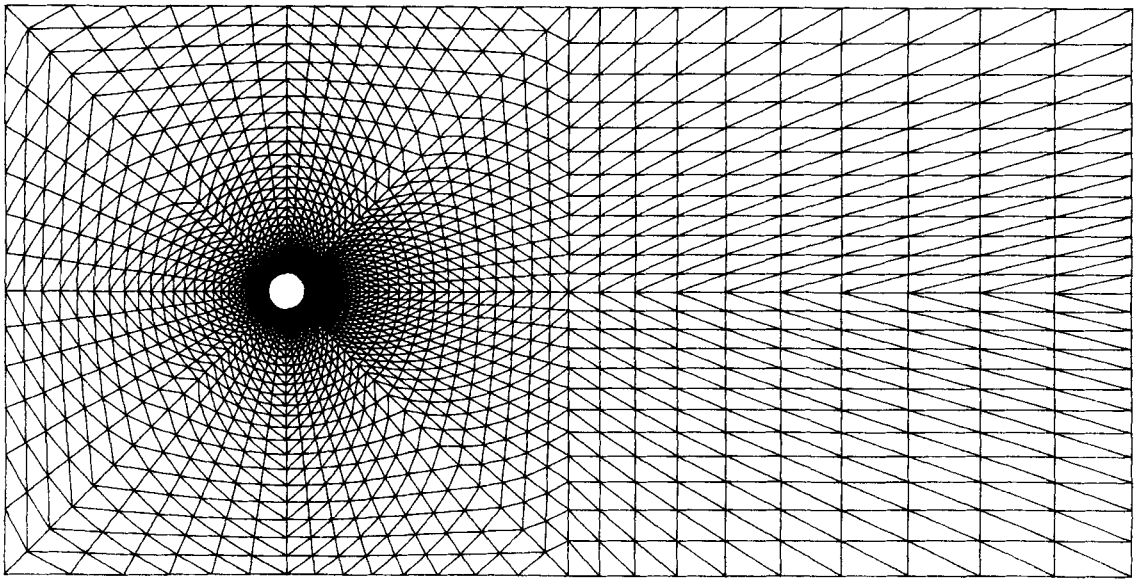

Figure 12. Subdivision of the domain for higher Reynolds numbers

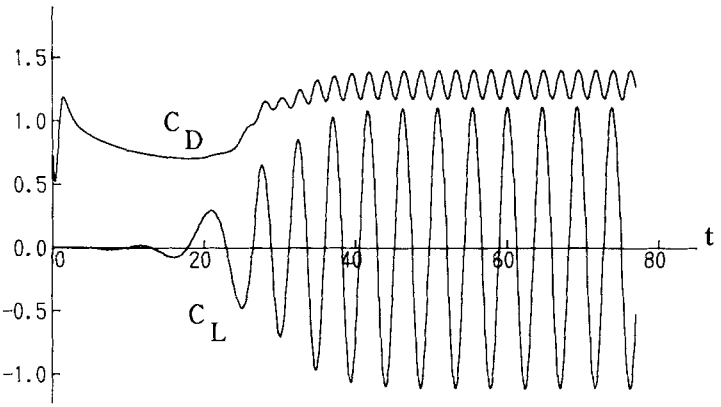

Figure 13. Time histories of C_D and C_L; $Re=1000$

gradually afterwards and finally the Karman vortex sheddings appear. Figure 19 depicts the time history of $\log_{10}|C_L|$. Setting

$$L(t)=\max\{|C_L(t')|;\quad 0\leqslant t'\leqslant t\},$$

we observe that the quantities $\log_{10}L(t)$ are almost linearly increasing, except for short initial time intervals in both computations, even while the variations in Figure 18 are decreasing. From Figure 19 we can read off

$$L_s(t)\simeq 10^{0\cdot 023t-4\cdot 1},\qquad L_d(t)\simeq 10^{0\cdot 023t-13\cdot 8},$$

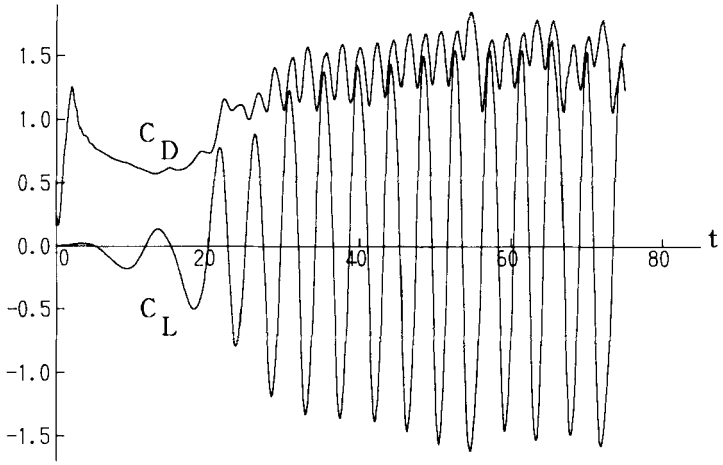

Figure 14. Time histories of C_D and C_L; $Re = 10000$

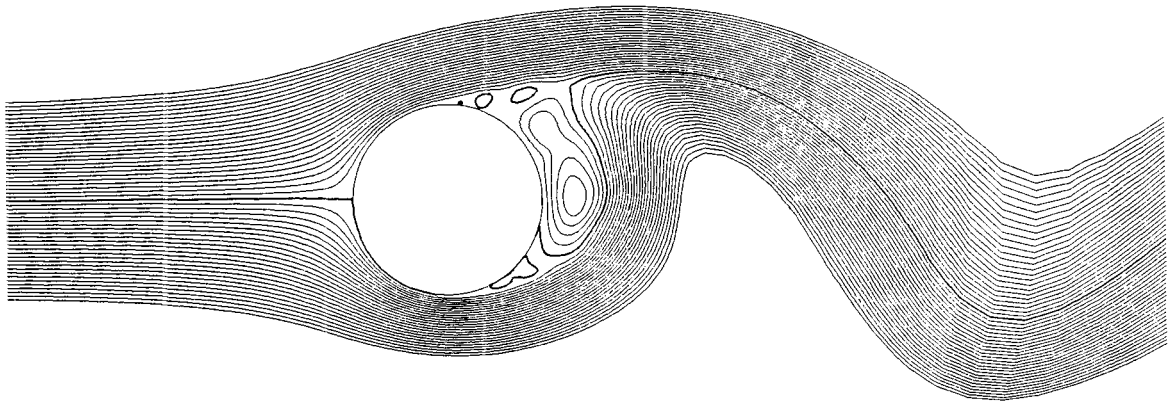

Figure 15. Streamlines; $Re = 10000$

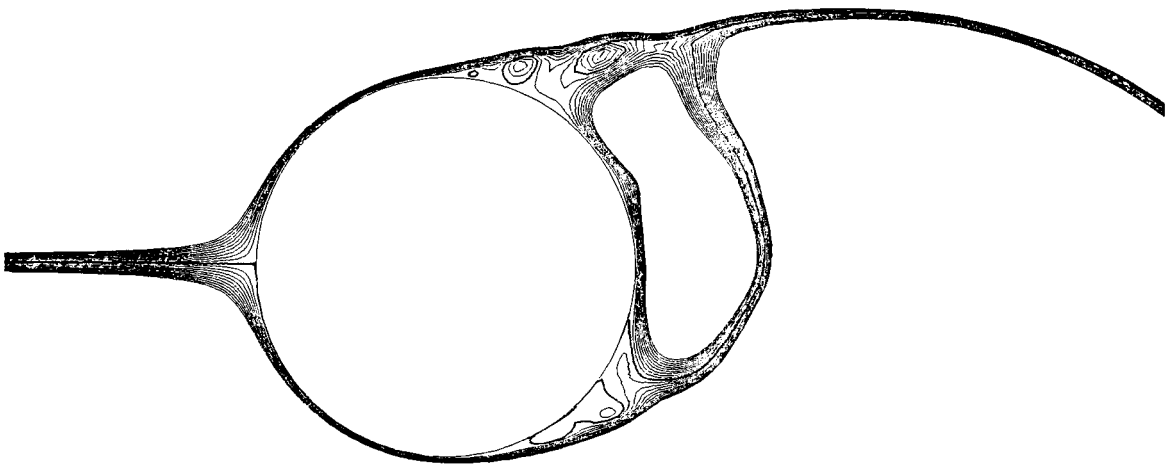

Figure 16. Detailed streamlines of Figure 15

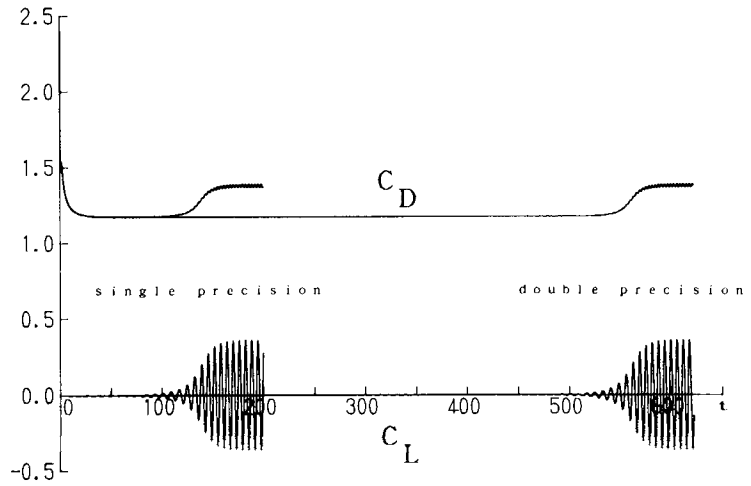

Figure 17. Time histories of C_D and C_L by single- and double-precision computations; $Re = 100$

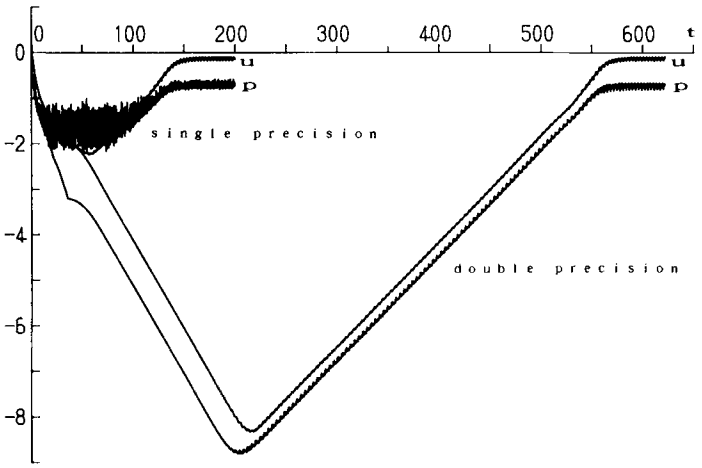

Figure 18. Variations of velocity and pressure; $Re = 100$

where the subscripts 's' and 'd' mean single-precision and double-precision respectively. Each $L(t)$ increases exponentially from the 'initial' disturbance, the size of which is dependent on the precision of computation. The increases stop when stable Karman vortex sheddings appear. Thus we see that C_L is a suitable quantity to characterize this phenomenon.

At $Re = 10$ the symmetric solution is stable. The disturbance caused by rounding errors does not grow and we obtain a stationary symmetric solution.

CONCLUDING REMARKS

We have presented a new upwind finite element scheme for the incompressible Navier–Stokes equations. It has the ability of approximating the convection term to third-order accuracy when

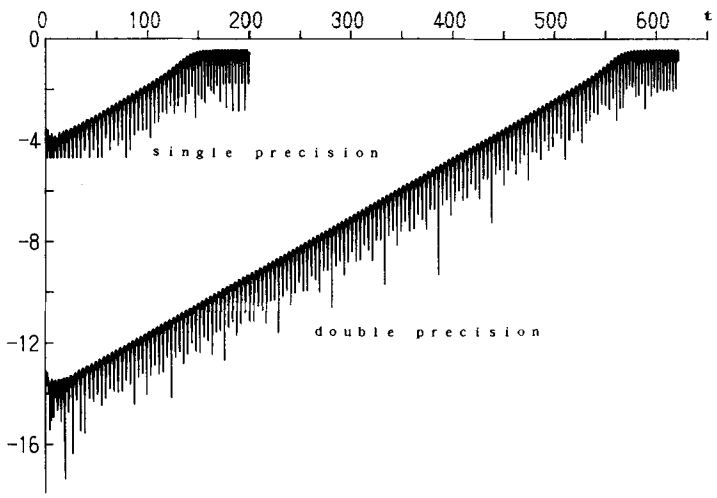

Figure 19. Time histories of log $|C_L|$ by single- and double-precision computations; $Re = 100$

upwind and downwind points are located suitably. The extension to three-dimensional problems is straightforward. The subdivision along the body, especially in the boundary layer, is recommended in order to obtain good numerical results. In the finite difference method one often uses the body-fitting co-ordinate system (called the generalized co-ordinate system) and solves the transformed Navier–Stokes equations on the grid of the transformed domain. On the other hand, we can realize such body-fitting decomposition by virtue of the freedom of the finite element subdivision and we do not need to introduce the generalized co-ordinate system. Therefore we have the advantage that the Navier–Stokes equations do not change from their original form.

Numerical results for model problems indicate the efficiency of this scheme for flow problems at high Reynolds numbers. Quantitative analysis, such as finding the critical Reynolds number of flow past a circular cylinder, is being investigated. We have also developed an efficient algorithm for the search of upwind and downwind points. These results will be reported elsewhere.

ACKNOWLEDGEMENT

The computations in this paper were carried out on the HITAC M-680H at the Computer Centre of the University of Tokyo.

REFERENCES

1. F. Thomasset, *Implementation of Finite Element Methods for Navier–Stokes Equations*, Springer, New York, 1981.
2. M. Tabata, 'A theoretical and computational study of upwind-type finite element methods', in T. Nishida *et al.* (eds), *Patterns and Waves*, Kinokuniya/North-Holland, Tokyo, 1986, pp. 319–356.
3. K. Ohmori and T. Ushijima, 'A technique of upstream type applied to a linear nonconforming finite element approximation of convective diffusion equations', *RAIRO Anal. Numer.*, **18**, 309–332 (1984).
4. B. P. Leonard, 'The QUICK algorithm: a uniformly third-order finite-difference method for highly convective flows', in K. Morgan, C. Taylor and C. A. Brebbia (eds), *Computer Methods in Fluids*, Pentech Press, London, 1980, pp. 159–195.
5. Y. Takemoto, H. Yamabe, Y. Abe and H. Naitou, 'On the third-order upwind finite-difference scheme in numerical analysis for initial-value problems', *IPPJ-693*, Institute of Plasma Physics, Nagoya University, 1984.
6. T. Kawamura, H. Takami and K. Kuwahara, 'New higher-order upwind scheme for incompressible Navier–Stokes equations', *Numerical Methods in Fluid Dynamics, Lecture Notes in Physics*, Vol. 218, Springer, Berlin, 1985, pp. 291–295.

7. T. Kawamura and K. Kuwahara, 'Computation of high Reynolds number flow around a circular cylinder with surface roughness', *AIAA Paper 84-0340, AIAA 22nd Aerospace Sciences Meeting*, 1984.
8. N. Kondo, N. Tosaka and T. Nishimura, 'High Reynolds solutions of the Navier–Stokes equations using the third-order upwind finite element method', in H. Niki and M. Kawahara (eds), *Proc. Computational Methods in Flow Analysis*, Okayama University of Science, Okayama, 1988, pp. 984–991.
9. J. C. Heinrich, P. S. Huyakorn, O. C. Zienkiewicz and A. R. Mitchell, 'An upwind finite element scheme for two-dimensional convective transport equation', *Int. j. numer. methods eng.*, **11**, 131–143 (1977).
10. V. Girault and P. A. Raviart, 'An analysis of upwind schemes for the Navier–Stokes equations', *SIAM J. Numer. Anal.*, **19**, 312–333 (1982).
11. A. Mizukami, 'Streamline-upwind/Petrov–Galerkin formulations for linear triangular elements', *Proc. 4th Int. Conf. on Numerical Methods in Laminar and Turbulent Flow*, Pineridge Press, Swansea, 1985, pp. 140–151.
12. A. Mizukami, 'Finite element analysis of two-dimensional viscous flows around a cylinder with particular emphasis on calculations of lift and drag', *Proc. 1st Symp. on Computational Fluid Dynamics*, Chuo University, Tokyo, 1987, pp. 219–222 (in Japanese).
13. T. J. R. Hughes and A. Brooks, 'A multi-dimensional upwind scheme with no crosswind diffusion', in T. J. R. Hughes (ed.), *Finite Element Methods for Convection Dominated Flows*, ASME, New York, 1979, pp. 19–35.
14. T. J. R. Hughes and A. Brooks, 'A theoretical framework for Petrov–Galerkin methods with discontinuous weighting functions: application to the streamline-upwind procedure', in R. H. Gallagher *et al.* (eds), *Finite Elements in Fluids*, Vol. 4, Wiley, New York, 1982, pp. 47–65.
15. M. Tabata, 'A finite element approximation corresponding to the upwind finite differencing', *Mem. Numer. Math.*, **4**, 47–63 (1977).
16. M. O. Bristeau, R. Glowinski, B. Mantel, J. Periaux, P. Perrier and O. Pironneau, 'A finite element approximation of Navier–Stokes equations for incompressible viscous fluids', in R. Rautmann (ed.), *Approximation Methods for Navier–Stokes Problems, Lecture Notes in Mathematics*, Vol. 771, Springer, Berlin, 1980, pp. 78–128.
17. P. M. Gresho, S. T. Chan, R. L. Lee and C. D. Upson, 'A modified finite element method for solving the time-dependent, incompressible Navier–Stokes equations, Part 1: Theory', *Int. j. numer. methods fluids*, **4**, 557–598 (1984).
18. P. M. Gresho and R. L. Sani, 'On pressure boundary conditions for the incompressible Navier–Stokes equations', *Int. j. numer. methods fluids*, **7**, 1111–1145 (1987).
19. J. F. Thompson, Z. U. A. Warsi and C. W. Mastin, *Numerical Grid Generation, Foundations and Applications*, North-Holland, Amsterdam, 1985.
20. M. Bercovier and O. Pironneau, 'Error estimates for finite element method solution of the Stokes problem in the primitive variables', *Numer. Math.*, **33**, 211–224 (1979).
21. V. Girault and P. A. Raviart, *Finite Element Methods for Navier–Stokes Equations, Theory and Algorithms*, Springer, Berlin, 1986.
22. P. G. Ciarlet, *The Finite Element Method for Elliptic Problems*, North-Holland, Amsterdam, 1978.
23. R. Verfürth, 'Error estimates for a mixed finite element approximation of the Stokes equations', *RAIRO Anal. numér.*, **18**, 175–182 (1984).
24. R. Stenberg, 'Analysis of mixed finite element methods for the Stokes problem: a unified approach', *Math. Comput.*, **42**, 9–23 (1984).
25. M. Tabata and S. Fujima, 'A finite element scheme for the Navier–Stokes equations using a third-order upwind approximation', in T. J. Chung and G. R. Karr (eds), *Finite Element Analysis in Fluids, Proc. 7th Int. Conf. on Finite Element Methods in Flow Problems*, University of Alabama in Huntsville Press, 1989, pp. 1034–1039.
26. U. Ghia, K. N. Ghia and C. T. Shin, 'High-*Re* solutions for incompressible flow using the Navier–Stokes equations and a multigrid method', *J. Comput. Phys.*, **48**, 387–411 (1982).
27. M. Nallasamy and K. K. Prasad, 'On cavity flow at high Reynolds numbers', *J. Fluid Mech.*, **79**, 391–414 (1977).
28. H. Schlichting, *Boundary-Layer Theory*, 7th edn., McGraw-Hill, New York, 1979.